Supporting Information for:

Directional and singular surface plasmon generation in chiral and achiral nanostructures demonstrated by Leakage Radiation Microscopy

Quanbo Jiang[1], Aline Pham[1], Martin Berthel[1],Serge Huant[1], Joel Bellessa[2], Cyriaque Genet[3] and Aurélien Drezet[1,*]

[1]*Université Grenoble Alpes, Institut NEEL, F-38000 Grenoble, France and CNRS, Institut NEEL, F-38042 Grenoble, France*

[2]*Institut Lumière Matière, UMR5306 Université Lyon 1-CNRS, Université de Lyon, 69622 Villeurbanne cedex, France*

[3]*ISIS, UMR 7006, CNRS-Université de Strasbourg, 8, allée Monge, 67000 Strasbourg, France*

[*]Corresponding author: aurelien.drezet@neel.cnrs.fr

Contents

1 Leakage radiation microscopy experimental setup

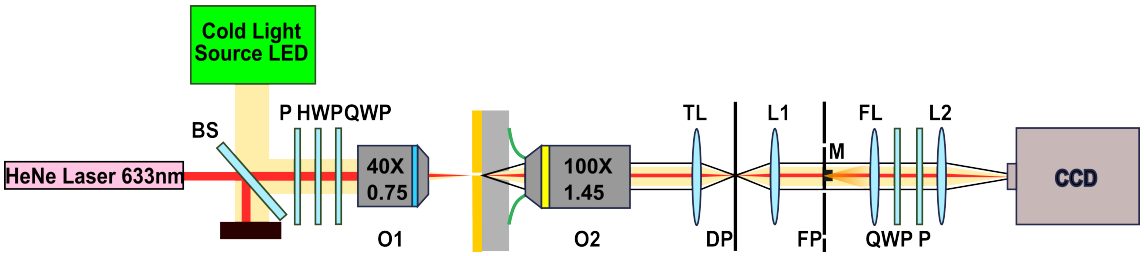

Figure 1: Leakage radiation microscopy setup. A normally incident laser beam is weakly focused onto the sample via a microscope objective O1. The leaky SPPs are collected by a CCD camera using an oil immersion objective O2. The input and output polarization states are prepared via a set of polarizer (P), half-wave plate (HWP) and quarter-wave plate (QWP). Fourier plane imaging is achieved by means of a Fourier lens (FL).

The SPP radiation images studied in this work were recorded via leakage radiation microscopy [1],[2]. The setup is depicted in Figure 1. A collimated He-Ne laser beam (633 nm) is weakly focused via a microscope objective (O1, $40\times, 0.75NA$) and normally illuminates the sample from the gold side. A cold light source LED is used to image and visualize the nanostructures on the sample. A set of polarizer (P), achromatic half-wave plate (HWP) and achromatic quarter-wave plate (QWP) is used to prepare the incident beam into the desired polarization state. Light which is scattered and transmitted through the glass substrate is collected with an oil immersion objective (O2, $100\times, 1.45NA$). The real plane images are focused onto the direct plane(DP) by means of a tube lens (TL, f=75mm). A lens (L1, f=75mm) projects that image on the Fourier plane (FP) where a beam blocker (M) can be used for spatially filtering the light directly transmitted through the sample. The real space image can also be mapped into the Fourier space via a Fourier lens (FL, f=75mm). A set of quarter-wave plate and polarizer is used to perform polarization analysis of the transmitted signals before they are focused via second lens (L2, f=150mm) onto a CCD camera.

2 Multidipolar representation of Λ- and T-shaped apertures

Here, we detail the analytical theory used in the letter. A model of two pairs of SPP dipoles is used to describe spin-controlled directional propagation of SPPs induced by Λ- and T-shaped apertures. In the proposed model, SPPs radiated by a rectangular aperture is approximately that of a in-plane pair of SPP dipoles formed by a major-axis dipole (orthogonal to aperture long axis) and a minor-axis dipole (orthogonal to aperture short axis).

On the one hand, let us consider the case of an elementary Λ-shaped structure. It is made of two rectangular apertures making an angle α with (Oy) and positioned at $\overrightarrow{x}_1 = (0,0)$ and $\overrightarrow{x}_2 = (-D,0)$ (see Figure 2(b)). The unit vectors of each dipoles are defined by $\widehat{n}_1 = (\cos\alpha, \sin\alpha)$, $\widehat{n}_{1\perp} = (-\sin\alpha, \cos\alpha)$, $\widehat{n}_2 = (-\cos\alpha, \sin\alpha)$, $\widehat{n}_{2\perp} = (\sin\alpha, \cos\alpha)$. An incident circularly polarized electric field $\overrightarrow{E}_\sigma = (\widehat{x} + i\sigma\widehat{y})/\sqrt{2}$ with handedness $\sigma = -1$ and $+1$ for right-handed circular polarization (RCP) and left-handed circular polarization (LCP) respectively excites the structure. The SPP dipole moment corresponding to the launched SPPs by each rectangular slit $(m = 1, 2)$ is given by:

$$\overrightarrow{\mu}_{m,\sigma} = \eta[(\overrightarrow{E}_\sigma \cdot \widehat{n}_m)\widehat{n}_m + \beta(\overrightarrow{E}_\sigma \cdot \widehat{n}_{m\perp})\widehat{n}_{m\perp}] \tag{1}$$

with:

$$\overrightarrow{\mu}_{1,\sigma} = \frac{1}{\sqrt{2}}\eta[(\cos\alpha + i\sigma\sin\alpha)\widehat{n}_1) + \beta(-\sin\alpha + i\sigma\cos\alpha)\widehat{n}_{1\perp}] \tag{2}$$

$$\overrightarrow{\mu}_{2,\sigma} = \frac{1}{\sqrt{2}}\eta[(-\cos\alpha + i\sigma\sin\alpha)\widehat{n}_2) + \beta(\sin\alpha + i\sigma\cos\alpha)\widehat{n}_{2\perp}] \tag{3}$$

where η is the polarizability of the major-axis dipole which depends on the geometry of the slit, β $(0 \leq \beta < 1)$ describes the weighted contribution of the minor-axis dipole with respect to the

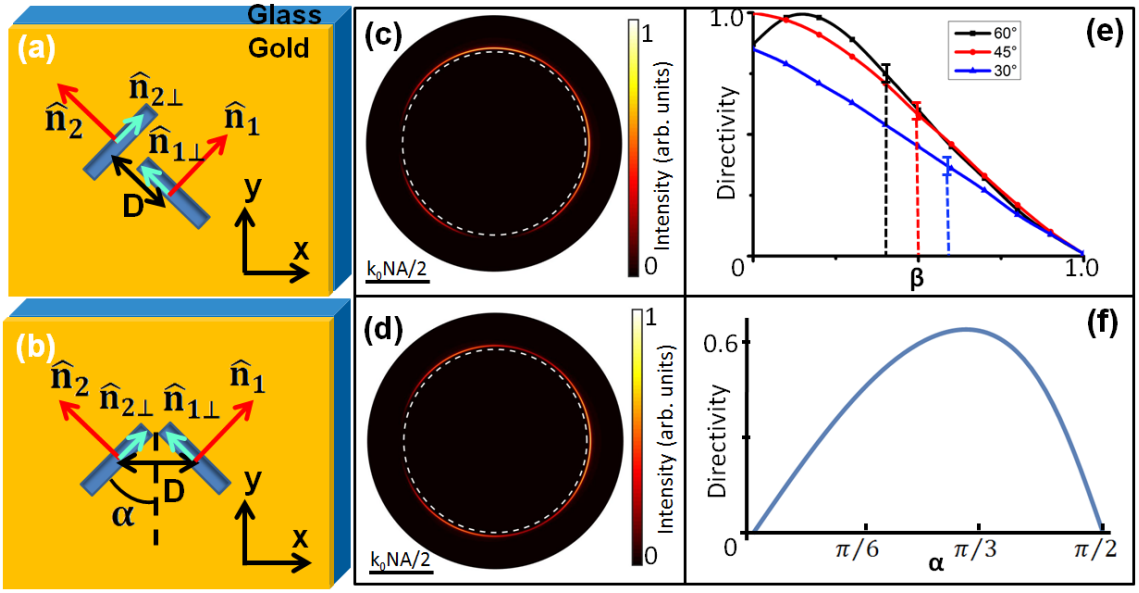

Figure 2: (a, b) Schematic diagrams of a T- and Λ-shaped aperture (top view). (c, d) Simulated results in Fourier space for a single T-shaped and Λ-shaped aperture taking $\beta = 0$, under the RCP excitation. (e) Theoretical plot of the directivity obtained for a Λ-shaped aperture as a function of β. The blue, red and black lines correspond to $\alpha = 30°$, $45°$ and $60°$ respectively. (f) Theoretical plot of the directivity as a function of α at given $\beta = 0.5$.

major-axis dipole in the SPP launching. In the Fourier plane, the radiated SPP field under an excitation field of σ is defined by:

$$\vec{E}_{\sigma}^{SPP}(k) = \sum_{m} \hat{k}(\vec{\mu}_{m,\sigma} \cdot \hat{k}) e^{i\Phi} F_{SPP}(k) \tag{4}$$

where $\vec{k}$ denotes the in-plane wavevector of the radiated light, $F_{SPP}(k) \simeq 1/(k - k_{SPP})$ defines the distribution of SPP radiated waves detected in the Fourier plane which has a Lorentzian lineshape, depicting the narrow ring like shape peaked at the SPP wave vector k_{SPP}. Owing to the strongly peaked resonance associated with $F_{SPP}(k)$ the spatial phase factor $\Phi = -\vec{k} \cdot \vec{x}_m$ now depends directly on the SPP wavevector k_{SPP} (assumed here to be a real number) such that $\Phi \approx -\vec{k}_{SPP} \cdot \vec{x}_m$. Inserting eq.2 and 3 in eq.4, the SPP field launched by a single Λ-shaped aperture along the direction of propagation $\hat{k}_{x\pm}$ becomes:

$$\vec{E}_{\sigma,\pm}^{SPP}(k) = F_{SPP}(k)[(\vec{\mu}_{1,\sigma} \cdot \hat{k}_{x\pm}) + (\vec{\mu}_{2,\sigma} \cdot \hat{k}_{x\pm}) e^{\pm i k_{SPP} \cdot D}] \cdot \hat{k}_{x\pm} \tag{5}$$

Assuming $k_{SPP} \cdot D = \pi/2$, the above equation simplifies as:

$$\vec{E}_{\sigma,\pm}^{SPP}(k) = \pm \frac{\eta}{\sqrt{2}} F_{SPP}(k) \cos^2\alpha \cdot C_{\sigma,\pm} \cdot \hat{k}_{x\pm} \tag{6}$$

where we introduce $C_{\sigma,\pm}$ which represents the coupling efficiency for RCP/LCP along $\hat{k}_{x\pm}$. It is given by:

$$C_{\sigma,\pm} = 1 \pm \sigma \tan\alpha + (\sigma \tan\alpha \pm 1)i + \beta[1 \mp \sigma \tan\alpha - (\sigma \tan\alpha \mp 1)i] \tag{7}$$

From $I_{\sigma,\pm}^{SPP} = \|\vec{E}_{\sigma,\pm}^{SPP}\|^2$ which is the SPP intensity in the Fourier space at the given direction of propagation and upon σ, we can deduce the directivity associated to a Λ-shaped aperture:

$$V_{\sigma} = \frac{|I_{SPP,\sigma,+} - I_{SPP,\sigma,-}|}{I_{SPP,\sigma,+} + I_{SPP,\sigma,-}} = \frac{2\beta(1-\beta)\tan^3\alpha + 2(1-\beta)\tan\alpha}{\beta^2\tan^4\alpha + (1+\beta^2)\tan^2\alpha + 1} \tag{8}$$

$I_{\sigma,\pm}^{SPP}$ for a single Λ-shaped aperture of infinitely thin width ($\beta = 0$) and under $\sigma = -1$ excitation is plotted in Figure 2(d). Here, the incident light that is directly transmitted through the sample

has been removed from the Fourier image.

On the other hand, in case of a single T-shaped aperture, we have $\overrightarrow{x}_1 = (0,0)$, $\overrightarrow{x}_2 = (-D/\sqrt{2}, D/\sqrt{2})$ and $\alpha = 45°$. Analogously, assuming $k_{SPP} \cdot D/\sqrt{2} = \pi/2$, eq.4 reduces as:

$$\overrightarrow{E}^{SPP}_{\sigma,\pm}(k) = \pm\frac{\eta}{2\sqrt{2}} F_{SPP}(k) \cdot C_{\sigma,\pm} \cdot \widehat{k}_{x\pm} \tag{9}$$

with

$$C_{\sigma,\pm} = 1 \pm \sigma + (\sigma \pm 1)i + \beta[1 \mp \sigma - (\sigma \mp 1)i] \tag{10}$$

Thus, the directivity for a single T-shaped aperture is followed by:

$$V_\sigma = \frac{1-\beta^2}{1+\beta^2} \tag{11}$$

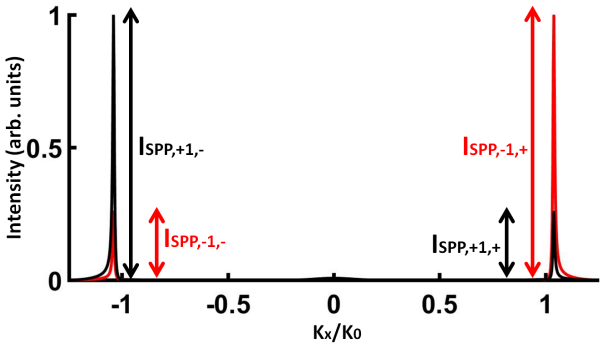

Figure 3: Intensity cross-section profiles along center line on Fourier image T-shaped apertures as indicated in Figure 2(c)($\beta = 0.5$). The black and red lines correspond to an LCP and RCP excitation, respectively.

A plot of $I^{SPP}_{\sigma,\pm}$ in the Fourier space for a single T-shaped aperture of infinitely thin width ($\beta = 0$), and upon $\sigma = -1$ is provided in Figure 2(c). An intensity cross section is achieved along the center (yellow dashed) line and plotted in Figure 3 for both $\sigma = -1$ and $\sigma = +1$ (not shown here). In accordance with the experimental results, two side peaks corresponding to the leaky SPP signals are clearly visible. The black and red curves relates to the resulting SPP signals excited by $\sigma = +1$ and $\sigma = -1$, respectively. Noteworthy, the intensity of the SPPs propagating in directions other than Ox are significant in case of the an elementary Λ- and T-shaped apperture while they are strongly attenuated when the later are arranged in arrays with horizontal period of λ_{SPP} and with vertical period of $\lambda_{SPP}/2$ as fabricated in the letter.

3 Method for determination of minor-axis dipole weight β

This part is devoted to the presentation of the method used to determine the contribution of the minor-axis dipole exhibited by the fabricated plasmonic structures. To do so, Λ-shaped aperture arrays with the aforementionned periods are fabricated with different angle $\alpha = 30°$, $\alpha = 45°$ and $\alpha = 60°$. They are analyzed in the Fourier space in which directivities are measured from intensity cross sections along the central line. We find directivities of 0.32 ± 0.11, 0.59 ± 0.09 and 0.74 ± 0.07 for $\alpha = 30°$, $\alpha = 45°$ and $\alpha = 60°$, respectively. Then, we plot V_σ obtained theoretically in eq.8 as a function of β for different angles $\alpha = 30^\circ, 45^\circ, 60^\circ$ as shown in Figure 2(e). From the directivities obtained experimentally, we thus deduce $\beta = 0.5 \pm 0.09$. Noteworthy, the presented error was calculated from the intensity cross section values obtained for different locations near the central line of the Fourier image. This explains the obtained high accuracy which however does not take into account any experimental uncertainties such as misalignment, polarizer imperfections. Additionally, despite the fact that the agreement between our theoretical and experimental results allows us to infer the validity of our model, our analytical study based on

multi-dipolar approximation has its limitations due to the finite size of the slits and to inter-dipole interactions that have been neglected.

In Figure 2(f), the directivity as a function of the angle α is plotted for a given $\beta = 0.5$. In agreement with the experimental directivity as well as previous theoretical works [3], the directivity of the Λ-shaped apertures takes its maximum value for $\alpha \approx 60°$.

4 Directional propagation of SPPs induced by an array of T-shaped apertures and its mirror image

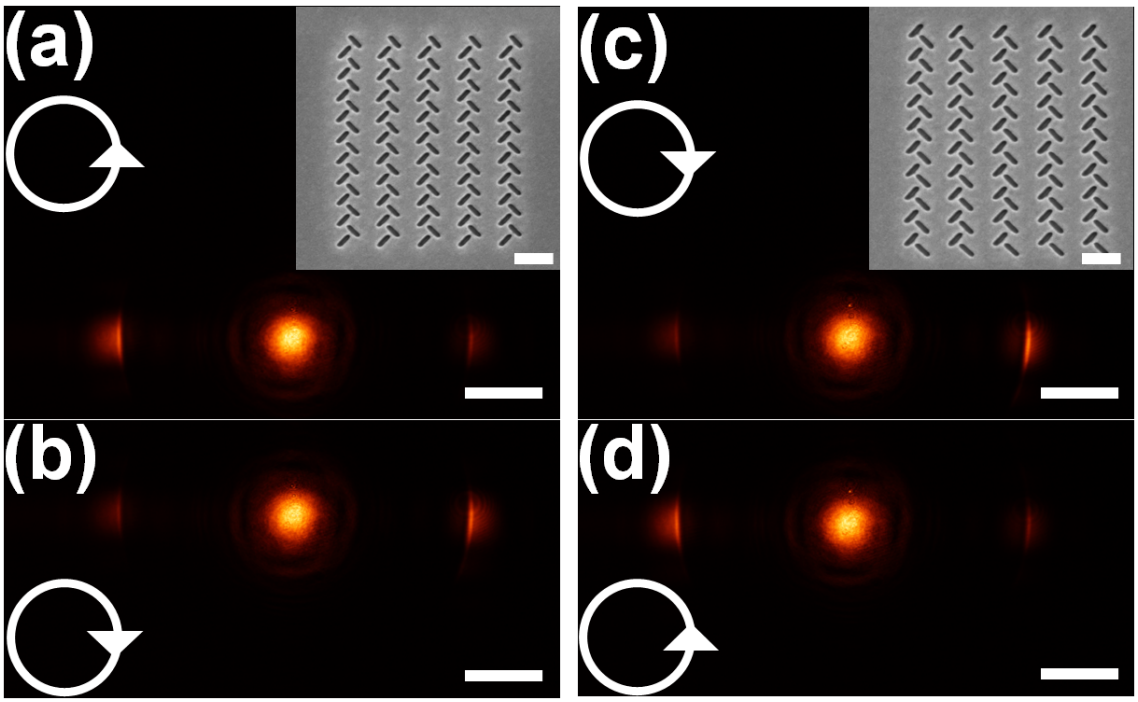

Figure 4: Fourier plane images (scale bar value $0.5k_0NA$) recorded by LRM for T-shaped apertures arrays (a, b) tilted to the left and (c, d) tilted to the right and illuminated by circular polarized beam as indicated by the white arrows. The insets in (a), (c) are SEM images of the plasmonic systems (scale bar value 600 nm).

In this part, the experimental results showing directional propagation of SPPs induced by an array of T-shaped apertures and its mirror image are provided. Scanning electron microscope images of the plasmonic structures are displayed in inset in Figure 4 along with Fourier plane images obtained by LRM. We show that a mirror symmetry reasonning can predict the directional property of chiral plasmonic structures and when combined with our multi-dipole model, it allows a full description of the T-shaped structures and its mirror image.

Indeed, from Figure 4(a), we can simply deduce the direction of propagation of SPPs in Figure 4(c) based on a mirror symmetry approach: an array of left-tilted T-shape apertures upon LCP leads to SPP propagating predominantly to the left direction (Figure 4(a)) whereas the symmetrical array is expected to induce SPP propagating towards the right direction upon RCP excitation (Figure 4(c)). However, no conclusion can be drawn about the resulting SPP directional coupling efficiency induced by the left-tilted T-shaped apertures arrays illuminated with RCP from the experimental results obtained in Figure 4(a).

We have analytically shown that using a description by a two-pairs of dipoles, a properly designed Λ-shaped element can exhibit identical directional coupling efficiency as a right tilted T-shaped aperture (Figure 4(c)). Similarly to a Λ-shaped element excited by RCP beam, we thus conclude that the right tilted T-shaped aperture (Figure 4(c)) leads to SPPs propagating towards the right

direction. Subsequently, by mirror symmetry, the left tilted T-shaped aperture (Figure 4(c)) leads to SPPs propagating towards the left direction.

5 Multidipolar representation of a set of T-shaped apertures arranged into a circle

The aim of this section is to provide the detailed derivations of the total SPP intensity generated by a plasmonic structure made of T-shaped apertures arranged in a ring configuration.

Let us first come back to a plasmonic structure comprising two rectangular slits refered here as A and B and oriented to form a T-shape. It is schematized in Figure 5(a). Each aperture is characterized by a short and long axis. The normal vectors to the long axis $\widehat{n}_i$ $(i = A, B)$ of each apertures are given by: $\widehat{n}_A = \dfrac{\widehat{U}_x + \widehat{U}_y}{\sqrt{2}}$ and $\widehat{n}_B = \dfrac{-\widehat{U}_x + \widehat{U}_y}{\sqrt{2}}$.

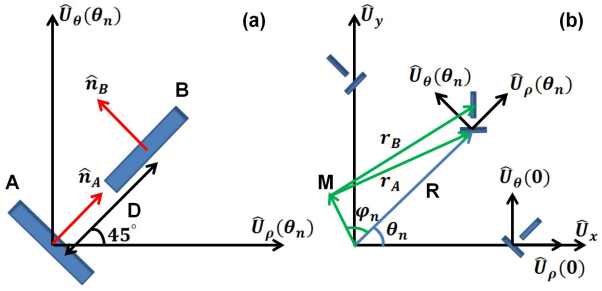

Figure 5: Chiral plasmonic structure. (a) Schematic of T-shaped nanoaperture. (b) T-shaped arranged in circle.

For the sake of simplicity, we consider a single dipole description for describing the SPP launched by a rectangular slit. Given that only the component of the incident light that is polarized perpendicularly to scattering elements can efficiently be coupled into SPPs, we here consider that the SPPs are mainly induced by SPP dipoles $\overrightarrow{\mu}_i$ along $\widehat{n}_i$.
Each T-shape elements are then duplicated and arranged in a ring configuration as displayed in Figure 5(b). The coordinate system associated to each elementary T aperture n comprising the plasmonic structure is referred as $(0, \widehat{U}_\rho(\theta_n), \widehat{U}_\theta(\theta_n))$. The plasmonic structure is excited by an incident electric field prepared in circular polarization state. In polar coordinates $(0, \widehat{U}_\rho(\theta_n), \widehat{U}_\theta(\theta_n))$, it writes:

$$\mathbf{E}_\sigma = \frac{e^{i\sigma\theta_n}}{\sqrt{2}}(\widehat{U}_\rho(\theta_n) + i\sigma\widehat{U}_\theta(\theta_n)) \tag{12}$$

with $\sigma = +1$ refering to a incident beam prepared in LCP and $\sigma = -1$ in RCP. Therefore, the SPP dipole moment corresponding to each slit is thus given by: $\overrightarrow{\mu}_i(\theta_n) = \eta(\mathbf{E}_\sigma.\widehat{n}_i(\theta_n)).\widehat{n}_i(\theta_n)$.
Let us now derive the total SPP field near the center of the structure on the direct plane. It can be expressed as:

$$\overrightarrow{E_{SPP}}(M) \propto \sum_{n=0,1...N} \frac{e^{i\mathbf{k_{SPP}}.\widehat{r}_A}}{\sqrt{r_A}}(\overrightarrow{\mu}_A.\widehat{r}_A)\widehat{r}_A + \frac{e^{i\mathbf{k_{SPP}}.\widehat{r}_B}}{\sqrt{r_B}}(\overrightarrow{\mu}_B.\widehat{r}_B)\widehat{r}_B \tag{13}$$

with N the total number of T-shape apertures comprising the ring. As we are interested in the SPP intensity distribution near the origin of the system, it is assumed the distance between the observation point M and each T-shaped aperture to be much greater than the exciting wavelength, and the distance between the slits $R \gg D, \lambda$. Hence, under this approximation: $\widehat{r}_A \approx \widehat{r}_B \approx \widehat{U}_\rho(\theta_n)$ and projected on the $\mathbf{E}_\sigma$ basis $(0, \mathbf{E_{-1}}, \mathbf{E_{+1}})$, we find the total SPP field at M is given by :

$$\begin{aligned}\overrightarrow{E_{SPP}}(M) \propto C_\sigma\{e^{i(\sigma+1)\theta_M} \sum_{n=0,1...N} e^{ik_{SPP}r_M cos(\varphi_M)} e^{i(\sigma+1)\varphi_M} \overrightarrow{E}_{-1} \\ + e^{i(\sigma-1)\theta_M} \sum_{n=0,1...N} e^{ik_{SPP}r_M cos(\varphi_M)} e^{i(\sigma-1)\varphi_M} \overrightarrow{E}_{+1}\}\end{aligned} \tag{14}$$

with

$$C_\sigma = n_A^x(0) + i\sigma n_A^y(0)).n_A^x(0) + n_B^x(0) + i\sigma n_B^y(0)).n_B^x(0)e^{ik_{SPP}D/\sqrt{2}} \tag{15}$$

Assuming $\theta_{n+1} - \theta_n \ll 1$, we can transform the sum into an integral:

$$\begin{aligned}\overrightarrow{E}^{SPP}(M) \propto C_\sigma\{e^{i(\sigma+1)\theta_M}(-1)^{\sigma+1}J_{\sigma+1}(k_{SPP}r_M)\overrightarrow{E}_{-1} \\ + e^{i(\sigma-1)\theta_M}(-1)^{\sigma-1}J_{\sigma+1}(k_{SP}r_M)\overrightarrow{E}_{+1}\}\end{aligned} \tag{16}$$

with $J_l(x)$ the l^{th} order Bessel function. Finally, we find the SPP intensity distribution after polarization analysis in RCP and LCP states in case of input state E_{-1} writes:

$$\begin{aligned}I_{RCP}^{E_{-1}}(M) \propto |C_{-1}|^2 J_0^2(k_{SPP}r_M) \\ I_{LCP}^{E_{-1}}(M) \propto |C_{-1}|^2 J_2^2(k_{SPP}r_M)\end{aligned} \tag{17}$$

and in case of input state E_{+1}:

$$\begin{aligned}I_{RCP}^{E_{+1}}(M) \propto |C_{+1}|^2 J_0^2(k_{SPP}r_M) \\ I_{LCP}^{E_{+1}}(M) \propto |C_{+1}|^2 J_2^2(k_{SPP}r_M)\end{aligned} \tag{18}$$

6 SPP radial propagation obtained by a left- and right-handed plasmonic structures

The results obtained for the plasmonic ring made of T shaped apertures are here compared to its mirror image. The LRM results are shown in Figure 6. The resulting fields are recorded upon incident circular polarized beam. No polarization analysis are performed here. As intituively anticipated, mirror symmetry property is conserved in the spin-dependent radial coupling. In case of the right-handed structure (Figure 6(a)), RCP illumination leads to inward directional coupling whereas for the left-handed structure (Figure 6(b)), it is obtained under LCP excitation. Inversely, we have outward directional coupling when the right-handed structure is excited with LCP illumination while it is obtained with RCP excitation for the left-handed structure.

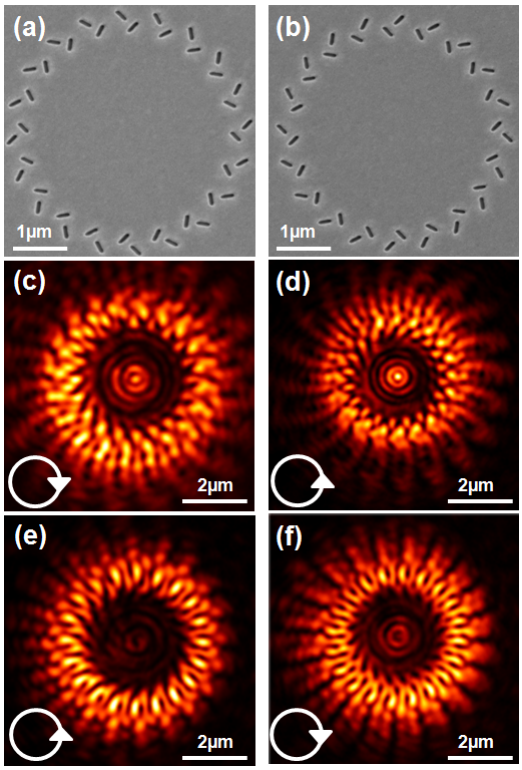

Figure 6: (a,b) SEM images of right-(a) and left-handed (b) plasmonic structures made of T shaped apertures.(c-f)LRM images obtained for the structures in (a) (first colunm) and in (b) (second column) upon circular polarized excitation as indicated by the white solid arrows.

As demonstrated in the paper, T and Λ shaped apertures feature comparable directionality in the x direction (Figures 2(a), (b)) when excited with circular polarization. This result is now extended to radial directionality when considering circular arrangement of these elements. In Figure7, we observe similar inward and outward propagation of SPPs as obtained for the ring consisting of T shaped apertures: in case of the right-handed structure (Figure 7(a)) a bright (respectively dark) spot is visible near the center of the structure under RCP (resp. LCP) excitation and inversely for the left-handed structure (Figure 7(b)) in accordance with the mirror symmetry. Further studies are under investigation in order to quantitatively compare and optimize the directional coupling induced by T and Λ shaped aperture based systems.

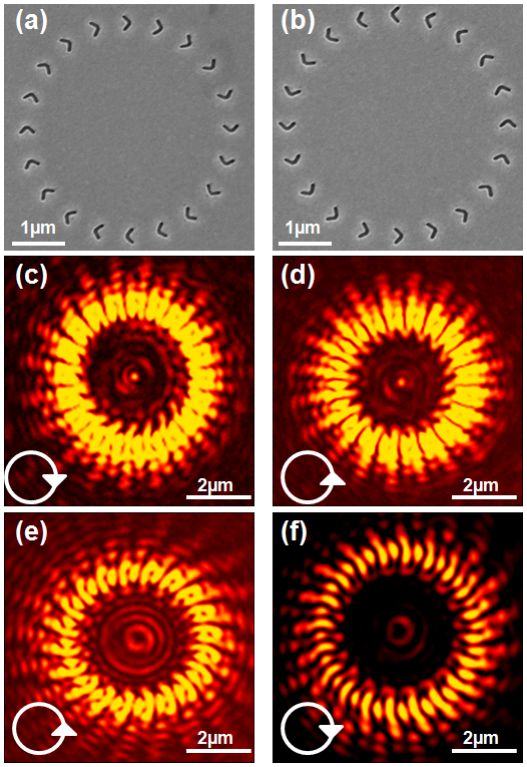

Figure 7: (a,b) SEM images of right-(a) and left-handed (b) plasmonic structures made of Λ shaped apertures. (c-f)LRM images obtained for the structures in (a) (first colunm) and in (b) (second column) upon circular polarized excitation as indicated by the white solid arrows.

References

[1] Drezet, A.; Hohenau, A.; Koller, D.; Stepanov, A.; Ditlbacher, H.; Steinberger, B.; Aussenegg, F.; Leitner, A.; Krenn, J. Leakage radiation microscopy of surface plasmon polaritons. *Mater. Sci. Eng. B* **2008**, 149, 220-229.

[2] Drezet, A.; Genet, C. Imaging Surface Plasmons: From Leaky Waves to Far-Field Radiation. *Phys. Rev. Lett.* **2013**, 110, 213901.

[3] Huang, F.; Yang, H. N.; Li, S. R.; Jiang, X. Q.; Sun, X. D. Tunable Unidirectional Coupling of Surface Plasmon Polaritons Utilizing a V-Shaped Slot Nanoantenna Column. *Plasmonics* **2015**, 10, 1825-1831.